Chitosan-magnetite nanocomposite as a sensing platform to bendiocarb determination

Raissa C. de Oliveira [1] · Camila P. Sousa [1] · Tiago M. Freire [1] · Rafael M. Freire [2,3] · Juliano C. Denardin [2,3] · Pierre B. A. Fechine [1] · Helena Becker [1] · Simone Morais [4] · Pedro de Lima-Neto [1] · Adriana N. Correia [1]

Abstract

A novel platform for carbamate-based pesticide quantification using a chitosan/magnetic iron oxide (Chit-Fe_3O_4) nanocomposite as a glassy carbon electrode (GCE) modifier is shown for an analytical methodology for determination of bendiocarb (BND). The BND oxidation signal using GCE/Chit-Fe_3O_4 compared with bare GCE was catalyzed, showing a 37.5% of current increase with the peak potential towards less positive values, showing method's increased sensitivity and selectivity. Using square-wave voltammetry (SWV), calibration curves for BND determination were obtained ($n = 3$), and calculated detection and quantification limits values were 2.09×10^{-6} mol L^{-1} (466.99 ppb) and 6.97×10^{-6} mol L^{-1} (1555.91 ppb), respectively. The proposed electroanalytical methodology was successfully applied for BND quantification in natural raw waters without any sample pretreatment, proving that the GCE/Chit-Fe_3O_4 modified electrode showed great potential for BND determination in complex samples.

Keywords Bendiocarb · Magnetic nanoparticles · Nanocomposite · Chitosan · Electrochemical sensor

Introduction

Carbamate compounds are the most used pesticides in agriculture due to their elevated insecticidal activity [1]. Bendiocarb (2,2-dimethyl-1,3-benzodioxol-4-ol methylcarbamate, BND) is classified as a broad spectrum pesticide and is highly toxic for humans if ingested or absorbed through the skin [2]. Notwithstanding the indiscrimination use, carbamate pesticides can bioaccumulate in natural sources with subsequent biomagnification throughout the food chain [3, 4]. The accumulation of BND in human body threatens health due to an interaction with acetylcholinesterase (AChE), an enzyme essential for a central nervous system function in humans [1, 2]. Being BND very dangerous and toxic to human health, their detection has a great importance among our life quality.

The detection and quantification of BND can be carried out by chromatographic methods, such as gas chromatography [4–6] and high-performance liquid chromatography (HPLC) [7–9]. Also, spectrophotometric [10] and fluorescence spectroscopy [11] methods are found in literature. However, some of these techniques are time consuming and often require expensive instrumentation and toxic reagents for sample preparation, making them complicated and thus unsuitable for field routine operation. Meanwhile, electrochemical techniques present advantages over the traditional analytical methods, such as low-cost instrumentation, accessible operation, fast response, and high sensitivity [12, 13].

Nevertheless, only a few studies regarding the electrochemical detection of BND have been reported. Hitchman et al. developed an electrochemical methodology for BND determination in soil samples using differential pulse polarography [14], for this methodology a calibration plots were linear over the range 4.49×10^{-5} to 2.24×10^{-4} mol L^{-1} in

✉ Camila P. Sousa
pinheiro.cs@gmail.com

1   Departamento de Química Analítica e Físico-Química, Centro de Ciências, Universidade Federal do Ceará, Bloco 940, Campus do Pici, Pici, Fortaleza, CE 60440-900, Brazil

2   Departamento de Física, Universidade de Santiago de Chile, Av. Ecuador, 3493 Santiago, Chile

3   Center for the Development of Nanoscience and Nanotechnology (CEDENNA), 917-0124 Santiago, Chile

4   REQUIMTE-LAQV, Instituto Superior de Engenharia do Porto, Instituto Politécnico do Porto, R. Dr. António Bernardino de Almeida 431, 4200-072 Porto, Portugal

an acetate buffer of pH 5.0. Guiberteau et al. studied the hydrolysis product of BND by differential pulse and square-wave voltammetries using a bare glassy carbon electrode (GCE) [15] obtaining a linear range of 2.24×10^{-6} to $1.07 \times 10^{-4} \ mol \ L^{-1}$ in an $0.5 \ mol \ L^{-1}$ NaOH. Regarding the BND hydrolysis, Rao et al. proposed the use of boron-doped diamond electrodes as a working electrode in an amperometric detector in HPLC separation to evaluate the electrochemical current of BND hydrolysis product along other two carbamates [16].

Many molecules in electroanalytical studies shows some issues, such as slow electron transfer reaction and electrochemical adsorption in working electrode due to oxidation/reduction subproducts, which reduces electrochemical area and decreases the sensibility [12, 17]. In this context, the application of metal nanoparticles as mediators has been the subject of growing interest in many fields of science, because their physical and chemical properties significantly differs from their microscopic metallic phases (or "bulk" phases) [18]. In this context, magnetic metal nanoparticles have been used in order to separate or concentrate analytes or controlling electrochemical reactions at electrode surface. The incorporation of this kind of metal nanoparticle associated with separation and detection capabilities created unique opportunities to improve the performance of the detection devices, in terms of selectivity and sensibility [19].

Among the several magnetic materials reported in the literature for analytical detection [20–30], iron oxides (mainly Fe_3O_4) nanoparticles are the most used due to its simple preparation and superparamagnetic properties [31–36]. Iron oxide nanoparticles can be applied for simple adsorption of biomolecules [37], functionalized and/or encapsulated with polymers or silica materials for making hybrid composites, providing increased functionality [38] and biocompatibility [39]. Chitosan (Chit), as a natural polymer with abundant primary amino groups and hydroxyl groups, is atoxic and have several properties, including hydrophilicity, good permeability, cost-effectiveness and availability of reactive functional groups for chemical modifications [40]. Because of its desirable and potentially synergic properties, chitosan has been combined with Fe_3O_4 nanoparticles in electrochemical sensing platforms for bisphenol A [41], urea [42], tetracycline [43], trichloroacetic acid [44], serotonin [45], and morphine [46].

Thus, in this work, the advantages of combining Chit and Fe_3O_4 in a nanocomposite were explored to develop and optimize a rapid, simple, accurate, and low-cost sensitive electrochemical approach for BND analysis based on a modified electrode. Furthermore, the analytical performance of GCE/Chit-Fe_3O_4 was assessed in natural raw waters without any sample pretreatment and compared with the reference method.

Experimental

Materials

Chitosan (DPN—Delta Produtos Naturais Ltda), ferric chloride hexahydrate ($FeCl_3 \cdot 6 \ H_2O$, 97%) and glacial acetic acid (CH_3COOH, 99.7%) were purchased from VETEC. Ferrous sulfate heptahydrate ($FeSO_4 \cdot 7H_2O$, 99%) and ammonium hydroxide solution (NH_4OH, 30%) were purchased from DINAMICA and Bendiocarb (PESTANAL®, analytical standard,) from Sigma-Aldrich. All reagents presented in this paper were of analytical grade and used without purification procedure. All solutions were prepared using water purified by Milli-Q System (Millipore Corp., water resistivity 18 M Ωcm). BND standard solution was prepared every day by dissolving an appropriate quantity of the solid (purity higher than 99.9%) in absolute ethanol.

Apparatus

An Autolab PGSTAT 101 potentiostat (Metrohm-Eco Chemie, The Netherlands) controlled by a personal computer using the Nova version 1.11.2 software was used for data acquisition. When necessary, a Microanal B474 pH meter equipped with a $3.0 \ mol \ L^{-1} \ Ag_{(s)}/AgCl_{(s)}/Cl^{-}_{(aq)}$ glass combined electrode was used to verify the pH values solution. All electrodes were cleaned before starting the electrochemical experiments using a Quimis Q335D ultrasonic cleaner equipped with a heating bath. HPLC analyses were done on a Shimadzu instrument equipped with a LC-20AT high pressure pump, a SPD-M20A photodiode array detector, and Shim-pack CLC-ODS (M)® C18 (250×4.60 mm, with 5 μm particle size) column was used in chromatographic experiments. The micrographs were obtained using a HITACHI HT7700 TEM electron microscope operating at an accelerating voltage of 120 kV.

Sensor preparation

Chit-Fe_3O_4 composite were synthesized according to the methodology developed by our research group [47]. Fe_3O_4 suspension was prepared at a concentration of 1 mg mL^{-1} using $0.04 \ mol \ L^{-1}$ BR buffer (pH 6.0) and before of the use the suspension was sonicate in an ultrasound bath for 10 min.

The GCE (BASi, 3 mm of diameter) was carefully polished with 3 μm diamond paste and sonicated in ethanol absolute and water for 3 min. The modified electrode (GCE/Chit-Fe_3O_4) was prepared by drop casting 5 μL of the suspension previously described onto the electrode's surface. The solvent was allowed to evaporate at a room temperature, and the GCE/Chit-Fe_3O_4 electrode was stored in a desiccator when it was not in use.

For obtention of micrographs, the transmission electron microscopy (TEM) sample was dispersed in ethanol and deposited on 300 mesh carbon-coated copper grids. Subsequently, the deposited sample was completely allowed to dry before examination.

Electrochemical experiments

All electrochemical experiments were conducted in a three-electrode electrochemical cell composed of a bare or modified GCE (BASi, 3 mm diameter) as the working electrode, a Pt sheet as the auxiliary electrode, and an $Ag_{(s)}/AgCl_{(s)}/Cl^-_{(aq)}$ (saturated KCl) as the reference electrode without oxygen purge. Prior to each new potential scan, the solution was stirred for 1 min with N_2.

Electrochemical impedance spectroscopy (EIS) experiments were performed in the presence of 1.0×10^{-3} mol L^{-1} Fe $(CN)_6^{3-}$/Fe $(CN)_6^{4-}$ (1:1) in 0.1 mol L^{-1} KCl at a frequency range of 60 kHz to 100 mHz using amplitude perturbation of 5 mV and 0.22 V versus $Ag_{(s)}/AgCl_{(s)}/Cl^-_{(aq)}$ (saturated KCl) as DC potential.

The optimization of the proposed electroanalytical methodology, obtaining values for detection and quantification limits (LoD and LoQ, respectively) and evaluation of precision and accuracy were performed as described in the literature in our previous work [48, 49].

HPLC conditions

The chromatographic determination of BND was performed after a system optimization which started by using isocratic conditions on an HPLC/ultraviolet-visible spectrophotometry (UV-Vis), as described by US Environmental Protection Agency [50]. The mobile phase consisted of water and acetonitrile (70:30), at a flow rate of 1.0 mL min^{-1}. The injection volume was 20 μL, and the working wavelength for quantitative analysis was 254 nm. These experiments were performed to compare the results obtained with SWV using modified glassy carbon electrode. In the HPLC/UV-Vis analysis, the LoD and LoQ were calculated considering the standard deviation (S_b) from the average value of the y-intercept from an analytical curve obtained at low concentration of the BND ($n = 3$) and the slope of this curves [51, 52].

Sample preparation

To evaluate the applicability of the proposed methodology, natural water samples were analyzed using the proposed electroanalytical methodology for matrix effect evaluation. Those water samples were collected from Acarape do Meio dam and Gavião dam as described in the literature in our previous works [48, 53].

Results and discussion

Characterization of the modified electrode

Aiming an initial electrochemical characterization of GCE/Chit-Fe$_3$O$_4$ electrode, cyclic voltammetry (CV) and electrochemical impedance spectroscopy (EIS) were performed in order to verify any potential synergic properties between chitosan and Fe$_3$O$_4$. The voltammogram profiles of 1.0 mmol L^{-1} [Fe $(CN)_6$]$^{3-/4-}$ and 0.1 mol L^{-1} KCl using GCE and GCE/Chit-Fe$_3$O$_4$ are shown in Fig. 1.

It was possible to verify the typical reversible redox process in the voltammograms obtained in Fig. 1a [54], where the relatively large peak current intensity was obtained on GCE/Chit-Fe$_3$O$_4$ in comparison with the bare GCE, showing a 18% of peak current augmentation. The differences between peak potential anodic and peak potential cathodic ($E_{pa} - E_{pc}$) values for bare and modified electrode were 86 mV and 71 mV, respectively, indicating that all of the modified electrodes improved the reversibility of the [Fe $(CN)_6$]$^{3-/4-}$ redox couple. The increase in the peak current and the decrease in the difference between the anodic potential and the cathodic potential are consequences of the modification of the surface of the electrode. Thus, when incorporating the nanocomposite
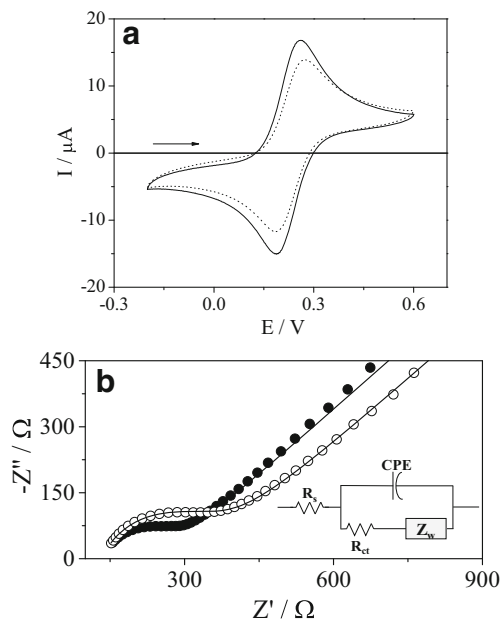
Fig. 1 **a** Cyclic voltammograms in 1.0 mmol L^{-1} [Fe $(CN)_6$]$^{3-/4-}$ containing 0.1 mol L^{-1} KCl on the GCE (dotted line) and GCE/Chit-Fe$_3$O$_4$ (solid line). Scan rate of 50 mV s^{-1}. **b** Nyquist plots of GCE (○○○) and GCE/Chit-Fe$_3$O$_4$ (●●●) in 1.0 mmol L^{-1} [Fe $(CN)_6$]$^{3-/4-}$ containing 0.1 mol L^{-1} KCl, with $f = 10$ kHz to 6 mHz, $a = 5$ mV, and $E_{dc} = 0.22$ V. The inserts correspond to the equivalent electrical circuit comprising the resistance of the solution (R_s/Ω), the Warburg impedance (Z_w/Ω), the double-layer capacitance (CPE/F), and the electron transfer resistance (R_{ct}/Ω)

on the surface, it was possible to verify a change in the catalytic effect as well as the increase of the electronic transfer rate [55, 56].

The electron transfer rate of materials was evaluated by EIS using the same electrochemical probe used in CV. The Nyquist plots shown in Fig. 1b display typical semi-infinite diffusion spectra for both bare and modified electrodes due to diffusion-controlled $[Fe\ (CN)_6]^{3-/4-}$ electrochemical reaction, and the semicircle length before the diffusion domain corresponds to the charge transfer resistance (R_{ct}), which reflects the electron transfer kinetics of the redox on electrode surface. The equivalent electrical circuit used to fit the electrochemical impedance data is also presented in an insert in Fig. 1b. The results are in agreement with those accomplished by CV (Fig. 1a). The calculated values of R_{ct} were 230 Ω and 133 Ω for GCE and GCE/Chit-Fe_3O_4, respectively. The results confirm that the GCE modification with Chit-Fe_3O_4 promotes the charge transfer as a result of the extraordinary conductivity of Fe_3O_4 and the catalytic activity accomplished from synergism concerning the chitosan and Fe_3O_4 nanoparticles [47, 57].

Figure 2a, b shows the TEM micrographs for the magnetic nanocomposite at different magnifications. One can be observe a presence of two distinct morphology: rods and spherical. It is interesting to note that the nanorod morphology is not present in the previous work [47, 58–60]. Thus, this result suggesting that the increase in the ultrasound time may lead to the formation of nanorods of magnetite coated with chitosan. Other authors have also showed that the increase in the ultrasonication time may change the shape of the magnetite nanoparticles [58]. Li et al. [58] showed that this changes occur when the time is increasing of 5 min to 30 min. Furthermore, Neto et al. [59] have synthesized magnetite ferrofluid with different polymers in a time greater than that used in this work and the nanoparticles do not present nanorods morphology. It is well-known that capping agent can orient the preferential growth of a crystal due to the change of the free energy of different facets [60]. Thus, the formation of magnetite nanorods may be due to the two main factors: (a) ultrasound time and (b) the free energy minimization due the interaction of the chitosan with magnetite crystal surface.

Electrocatalytic behavior of the BND

The electrochemical behavior of BND on a bare and modified electrode was investigated by square-wave voltammetry (SWV) using default parameters values ($f = 100\ s^{-1}$, $a = 50$ mV, and $\Delta E_s = 2$ mV) in BR buffer pH 3.0, Fig. 3.
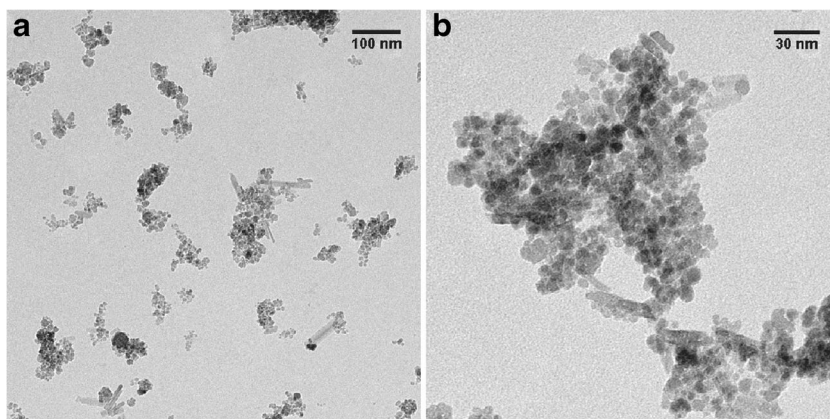
The square-wave voltammogram obtained present an oxidation process at $+1.37$ V for bare GCE and $+1.35$ V. For both electrodes, the reverse current is negligible, a characteristic behavior of irreversible processes. Along with peak potential shift towards less positive potentials, the peak current for BND oxidation if compared with bare GCE increased 37.5%, demonstrating the catalytic effect of modified GCE/Chit-Fe_3O_4 electrode if compared with bare GCE.

Optimization studies

Effect of pH and supporting electrolytes

The pH effect over the 2.91×10^{-5} mol L^{-1} BND oxidation was studied using SWV and GCE/Chit-Fe_3O_4 modified electrode in 0.1 mol L^{-1} Britton-Robinson buffer at pH range between 3.0 and 7.0. The square-wave voltammograms in each pH value are shown in Fig. 4a. The maximum current appeared at pH 3.0 for BND oxidation, being 3.0 the optimized pH value. Furthermore, the dependence between both peak current and peak potential versus pH are shown in Fig. 4b, and it was possible to observe that the peak potential values declined linearly with increasing pH, indicating the participation of protons

Fig. 2 **a**, **b** TEM images (at different magnifications and regions) of Chit-Fe_3O_4 magnetic nanocomposites with two distinct morphologies
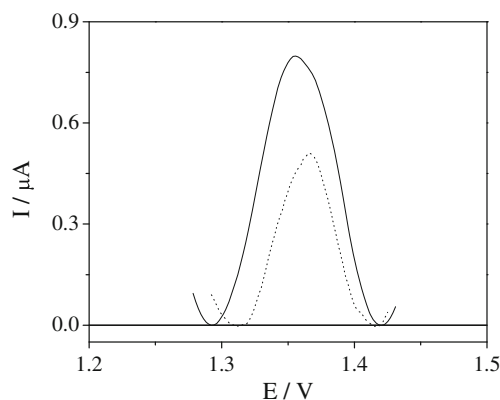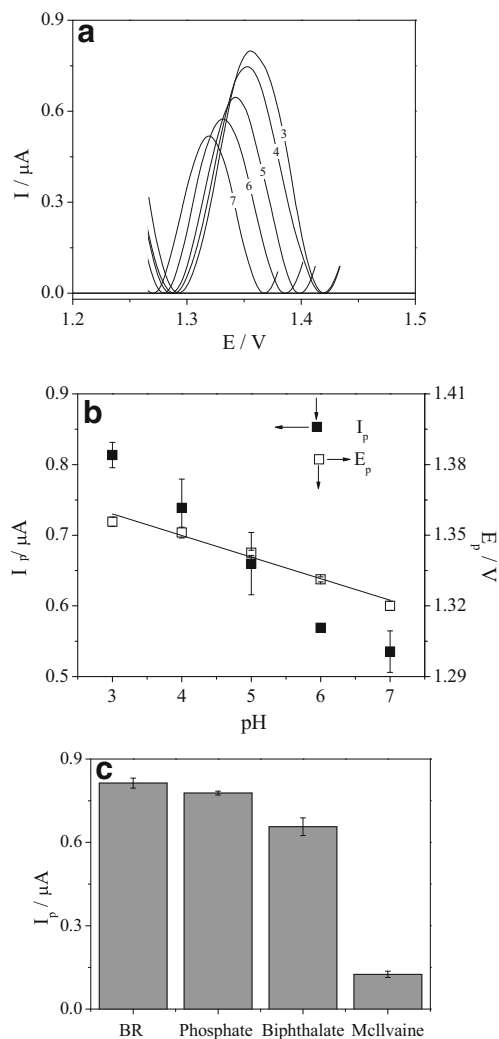
Fig. 3 Square-wave voltammograms for [BND] = 2.91×10^{-5} mol L^{-1} in BR buffer pH 3.0 on the GCE (dotted line) and GCE/Chit-Fe$_3$O$_4$ (solid line) with f = 100 s^{-1}, a = 50 mV, ΔE_s = 2 mV, E_{acc} = 1.15 V, and t_{acc} = 60 s

in the BND oxidation. The linear equation (E_p = 1.3955–0.0107 pH) presented a slope different to the theoretical value predicted by the Nernst equation, 0.059 V/pH [61], proposing that there is the involvement of a different number of protons and electrons. Also, the current throw down when pH increases due outstanding to BND hydrolysis, once the oxidation signal is related with BND molecule without hydrolysis. The presence of non-hydrolyzed BND decreases when pH increases, BND is an ester, and hydrolysis is favored breakdown goes in basic medium. The proposed mechanism is shown in Scheme 1, being this mechanism based on the mechanism of the BND metabolism proposed by Croucher and coauthors [62] for situations where the hydrolysis of BND does not occur already reported by different authors [15, 16, 63].

The influence of supporting electrolytes was also analyzed by SWV in the same conditions as shown before. The selected buffers were 0.04 mol L^{-1} Britton-Robinson buffer, 0.1 mol L^{-1} phosphate buffer, biphthalate buffer, and McIlvaine buffer solution. The anodic peak current for BND oxidation for all electrolytes were compared at the same pH value, 5.0. The mean peak currents obtained by SWV for BND oxidation in each described buffer solution are shown in Fig. 4c. The maximum absolute peak current was obtained with 0.04 mol L^{-1} BR buffer. Thus, 0.04 mol L^{-1} BR buffer was chosen as optimized supporting electrolyte.

Effect of accumulation

The accumulation potential (E_{acc}) effect on the oxidation peak current of BND were investigated on GCE/Chit-Fe$_3$O$_4$ modified electrode using 0.04 mol L^{-1} BR buffer pH 3.0 as electrolyte at 2.91×10^{-5} mol L^{-1} BND. The selected potential interval was located between 0.60 and 1.25 V, and the oxidation of BND was studied by SWV using the following parameters: f = 100 s^{-1}, a = 50 mV,

Fig. 4 **a** Square-wave voltammograms for [BND] = 2.91×10^{-5} mol L^{-1} on the Chit-Fe$_3$O$_4$/GCE with f = 100 s^{-1}, a = 50 mV, ΔE_s = 2 mV, E_{acc} = 1.15 V, and t_{acc} = 60 s in BR buffer in different pH values. **b** Dependence between peak current (I_p) and peak potential (E_p) of [BND] = 2.91×10^{-5} mol L^{-1} versus pH values. **c** Peak current obtained by square-wave voltammograms for [BND] = 2.91×10^{-5} mol L^{-1} on GCE/Chit-Fe$_3$O$_4$ with f = 100 s^{-1}, a = 50 mV, ΔE_s = 2 mV, E_{acc} = 1.15 V, and t_{acc} = 60 s in different buffers all in pH 3.0
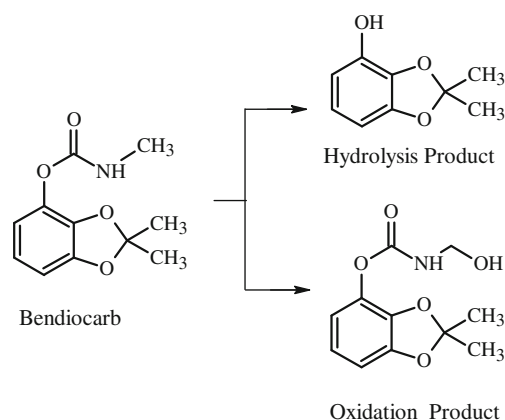
Scheme 1 Proposed mechanism for BND at GCE/Chit-Fe$_3$O$_4$

and $\Delta E_s = 2$ mV. The anodic peak currents of BND showed a linear dependence within the E_{acc} between the potential range between 0.60 and 1.15 V (data not shown), showing the E_{acc} influence over the BND oxidation, being 1.15 V the optimized E_{acc} value.

Regarding the accumulation time (t_{acc}), a time range between 0 and 120 s was applied in the same conditions for E_{acc} study. The t_{acc} increased gradually, reaching a maximum at $t = 60$ s and the anodic peak current remained constant after 60 s (data not shown). This effect can be attributed due to the adsorption of BND over the electrode surface and further BND saturation when higher accumulation times were achieved. Thus, 60 s was selected as the optimized accumulation time.

Voltammetric parameters

To achieve the maximum sensitivity in this proposed electroanalytical methodology, SWV parameters were evaluated in order to achieve an optimized value for frequency (f), amplitude (a), and step potential (ΔE_s). The method of optimization of the SWV was carried as follows: one of SWV parameters (f, a, and ΔE_s) changed their value while the other two remain constant. All experiments were conducted in triplicate. For frequency, a range between 10 and 150 s^{-1} was applied, and a linear dependence for both I_p and f and E_p and log (f) was observed between 10 and 80 s^{-1}. This double linear dependence is a characteristic behavior of electrochemical irreversible processes [17], which confirms the same conclusion shown earlier. For irreversible process, the half-height width higher than 40 mV is an adsorption indicative of the product and the reagent. In addition, for a value of $\alpha = 0.5$, $E_{p/2}$ is equal to $127/n$ [17], since the $E_{p/2}$ for the proposed system is 74.9 mV, the number of electrons involved in the BND oxidation are two electrons. After 80 s^{-1}, no linear correlation was achieved, and the optimized frequency was chosen as 80 s^{-1}.

For pulse amplitude (a), a range between 10 and 80 mV was studied, and a linear dependence between I_p and a was observed between 10 and 60 mV, and 60 mV was considered the optimized amplitude.

Regarding the step potential (ΔE_s), the considered range was between 1 and 5 mV, and no linear dependence between I_p and ΔE_s was found. Then, another criterion was taken as follows: a step potential was chosen so that it has the lowest half-height peak width, and 1 mV of step potential was chosen because met the criteria and was chosen as the optimized step potential. Therefore, the optimized parameters for the proposed methodology were $f = 80$ s^{-1}, $a = 60$ mV, $\Delta E_s = 1$ mV, $E_{acc} = 1.15$ V, and $t_{acc} = 60$ s.

Calibration, reproducibility, and repeatability

Calibration curves for BND were obtained using GCE/Chit-Fe$_3$O$_4$ sensor associated with the optimized electroanalytical methodology. Figure 5 presents the square-wave voltammograms for different BND concentrations, with an inset showing the linear correlation between I_p and BND concentration.

The calculated mean analytical curve was $I_p = -2.14 \times 10^{-7} + 0.06$ [BND] for the concentrations ranging from 4.97×10^{-6} to 3.01×10^{-5} mol L^{-1}. Since the linear coefficient of the analytical curve was negative, a statistical t test was applied to determine whether the linear coefficient of the analytical curve can be statistically considered equal to zero or if it should be used to the samples concentrations. The significance test was applied to the linear coefficient and the observed t value was 7.14, while the tabulated t value is 4.30 for a 95% confidence level which indicated that the linear coefficient cannot be considered as statistically equal to zero.

The methodology's repeatability was evaluated using only one modified electrode at the same BND concentration for seven consecutive measurements. The calculated relative standard deviation (RSD) was 1.83%. Moreover, five different electrodes were prepared and measured one BND concentration, and the calculated RSD was 2.76%, indicating that the proposed methodology showed good repeatability and reproducibility, and is potentially effectively applicable for analytical purposes. The analytical figures of merit are described in Table 1.

Table 2 presents an overview of methodologies used for the BND detection. The results achieved together with the high simplicity of the electrochemical sensors is favorably compared with other methods used. There is no methodology for BND detection based on modified electrodes,
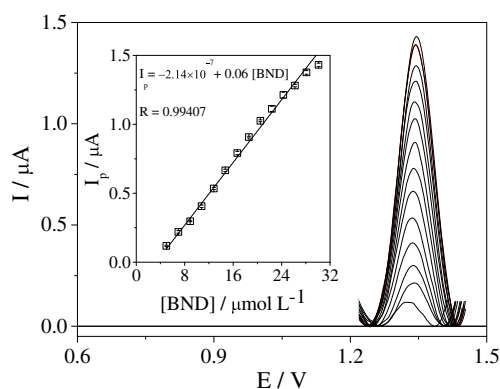
Fig. 5 Square-wave voltammograms for BND in 0.04 mol L^{-1} BR buffer at pH 3.0 on the GCE/Chit-Fe$_3$O$_4$ with $f = 80$ s^{-1}, $a = 60$ mV, $\Delta E_s = 1$ mV, $E_{acc} = 1.15$ V, and $t_{acc} = 60$ s in concentrations in the interval from 4.97×10^{-6} to 3.01×10^{-5} mol L^{-1} of BND. The insert shows the average current obtained from three analytical curves
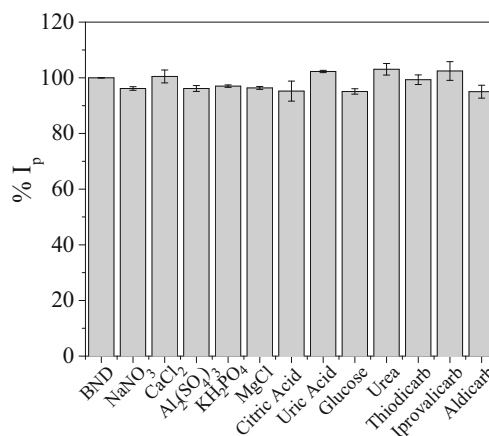
Table 1 Calculated analytical figures of merit for BND quantification using SWV

Parameter	SWV
Linearity range/mol L^{-1}	4.97×10^{-6}–3.01×10^{-5}
Intercept/A	-2.14×10^{-7}
Slope/A mol^{-1} L^1	0.06
Confidence interval of intercept/A	$\pm 5.42 \times 10^{-8}$
Confidence interval of the slope/A mol^{-1} L^1	$\pm 1.54 \times 10^{-3}$
Correlation coefficient	0.99407
SD of the intercept/A	4.79×10^{-9}
LoD/mol L^{-1}	2.09×10^{-6} (466.99 ppb)
LoQ/mol L^{-1}	6.97×10^{-6} (1555.91 ppb)
Repeatability	1.83 ($n = 7$)
Reproducibility	2.76 ($n = 5$)

Fig. 6 Interference of 100-fold concentration of NaNO$_3$, CaCl$_2$, Al$_2$(SO$_4$)$_3$, KH$_2$PO$_4$, MgCl, citric acid, uric acid, glucose, and urea and 10-fold concentration of thiodicarb, iprovalicarb, and aldicarb to the determination of BND in 0.04 mol L^{-1} BR buffer at pH 3.0 on the GCE/Chit-Fe$_3$O$_4$ with $f = 80$ s^{-1}, $a = 60$ mV, $\Delta E_s = 1$ mV, $E_{acc} = 1.15$ V, and $t_{acc} = 60$ s

making this a pioneering work. In relation to these studies, the value of the LoD calculated in this work is of the same order of magnitude as for the spectrophotometric [64], spectrofluorimetric [11], and electrochemical methodology of detection of hydrolysis products [15]. It is important to emphasize that the authors report a great adsorption of the compounds on the electrode surface which may compromise the reproducibility and applicability of the proposed methodology [15]. Despite the results obtained, the value of the LoD is higher orders of magnitude than that obtained by high-performance liquid chromatography with electrochemical detection, because these results are justifiable due to the preparation of the sample used [16].

Interference study

The insertion of potentially interfering chemicals over the anodic current peak of BND oxidation was evaluated using the proposed optimized electroanalytical methodology. The changes in anodic peak current of BND due to the presence of different salts and organic molecules 100 times more concentrated and different carbamates 10 times more

concentrated than BND are shown in Fig. 6. It can be seen almost no influence on the peak current responses of BND (signal changed below 5%). The obtained results clearly demonstrate the efficiency of the proposed electroanalytical methodology for the determination of BND, even in the presence of the potentially interfering species. In addition, it is important to note that even in the presence of other carbamates, the peak current obtained for the oxidation of BND was not altered, demonstrating that the developed methodology is selective for bendiocarb.

Analytical performance in water samples

In order to achieve a practical application of the proposed electroanalytical methodology for BND sensing, natural raw waters samples were collected for this purpose. As shown in Table 3, all samples were fortified with different concentrations of BND. The recovery percentage was calculated using the analytical curve previously obtained. For GCE/Chit-Fe$_3$O$_4$ modified electrode. The calculated values agreed with the assigned value for each sample. The calculated recovery

Table 2 Comparison of the proposed sensor for determination of BND with others methodologies described in the literature

Methodology	Linearity range/mol L^{-1}	LoD/ mol L^{-1}	Ref.
Spectrofluorimetry with hydroxypropyl-β-cyclodextrin	0–1.20×10^{-4}	2.55×10^{-6}	[11]
Differential pulse polarography	4.49×10^{-5}–2.24×10^{-4} mol L^{-1}	–	[14]
Square-wave voltammetry for formed hydrolysis products	2.24×10^{-6}–1.07×10^{-4} mol L^{-1}	1.97×10^{-6}	[15]
High-performance liquid chromatography with electrochemical detection	1.00×10^{-8}–1.00×10^{-5}	1.00×10^{-8}	[16]
Spectrophotometric	1.79×10^{-6}–6.27×10^{-5}	1.27×10^{-6}	[64]
Square-wave voltammetry	4.97×10^{-6}–3.01×10^{-5}	2.09×10^{-6}	This work

Table 3 Analytical parameters for BND recovered using SWV and HPLC procedures

Parameters	Gavião dam						Acarape do Meio dam					
	SWV			HPLC			SWV			HPLC		
$[BND]_{added}$/$\mu mol\ L^{-1}$	9.90	19.6	29.1	4.0	12	30	9.90	19.6	29.1	4.0	12	30
$[BND]_{found}$/$\mu mol\ L^{-1}$	8.35	16.69	25.15	4.16	11.3	28.3	7.22	16.21	25.23	4.28	12.6	27.3
Recovery (%)	84.4	85.18	86.44	103.98	94.10	94.20	72.98	82.74	86.71	107.09	105.21	90.98
RSD (%)	3.21	3.33	2.89	6.28	3.47	1.96	4.06	4.57	1.60	2.51	8.25	4.45
BIAS (%)	− 15.6	− 14.82	− 13.56	3.98	− 5.90	− 5.80	− 27.02	−17.26	−13.29	7.09	5.21	9.02

percentages for BND quantification using GCE/Chit-Fe$_3$O$_4$ electrode (from 72.98 to 86.71%) in natural raw water samples confirms the applicability and successfulness of the proposed electroanalytical method.

The physicochemical parameters shown in Table 4 were used to estimate the quality of the water samples which were used for BND quantification. The relationship of chlorophyll A with phosphorus and nitrogen concentration and optics (transparency) allows to characterize the degree of trophy of an aquatic system [65]. Although algae are a natural part of freshwater ecosystems, many of them can result in reduced levels of dissolved oxygen. Natural waters with high levels of fertilizer nutrients, septic systems, sewage treatment plants and urban runoff may have high concentrations of chlorophyll A [66]. Although the water samples showed a great complexity due of its composition, the analytical method was selective and robust to determine the BND directly in these waters.

The BND quantification was also analyzed by HPLC. The analysis of statistically significant difference of the two techniques showed that the results obtained with this sensor were in satisfactory agreement with data from the reference method for a 95% confidence level using the paired t test model. This result indicates that this sensor has good accuracy for BND detection in real samples.

Table 4 Physicochemical parameters for the raw natural waters, Gavião dam and Acarape do Meio dam

Parameters	Gavião dam	Acarape do Meio dam
Chlorophyll A ($\mu g\ L^{-1}$)	55.11	52.01
Total phosphorous (mg P L^{-1})	0.031	0.062
Organophosphate (mg P-PO$_4^{-3}$ L^{-1})	≤ 0.01	≤ 0.01
Total nitrogen ($\mu g\ L^{-1}$)	0.158	1.989
Ammonia nitrogen (mg N-NH$_3$ L^{-1})	≤ 0.1	≤ 0.1
NO$_2^-$ (mg N-NO$_2^-$ L^{-1})	≤ 0.005	≤ 0.005
NO$_3^-$ (mg N-NO$_3^-$ L^{-1})	≤ 0.035	0.047
Feofitin ($\mu g\ L^{-1}$)	14.79	42.93

Conclusions

The Chit-Fe$_3$O$_4$ was satisfactorily applied as electrode modifier for GCE, and the application for electrochemical determination for BND presented good sensitivity and analytical stability. The nanocomposite Chit-Fe$_3$O$_4$ which modified GCE electrode proved to have a synergistic effect over electrochemical reactions, bringing a peak current augmentation for both $[Fe(CN)_6]^{3-/4-}$ redox couple and BND oxidation. The proposed electroanalytical method exhibited outstanding sensitivity as well as good accuracy and precision. Regarding the BND determination, comparisons among the data acquired from the proposed electroanalytical method and HPLC data showed that the proposed electroanalytical procedure can be applied to quantify BND in natural raw water samples. This application is a consequence of the robustness of the electroanalytical technique, once the BND oxidation at GCE/Chit-Fe$_3$O$_4$ electrode presented almost no interference in anodic peak currents of BND, even in more complex samples, such as raw natural water samples.

Compliance with ethical standards

Conflict of interest The authors declare that they have no conflict of interest.

References

1. Kuhr RJ, Dorough HW. Carbamate insecticides: chemistry, biochemistry, and toxicology. CRC Press, Inc.; 1976.

2. Kamrin MA. Pesticide profiles: toxicity, environmental impact, and fate. CRC Press; 1997.

3. Wang QQ, Lemley AT. Competitive degradation and detoxification of carbamate insecticides by membrane anodic Fenton treatment. J Agric Food Chem. 2003;51:5382–90.

4. Szeto SY, Wilkinson ATS, Brown MJ. A gas-chromatographic method for the determination of bendiocarb in soil and corn—application to the analysis of residues in corn. J Agric Food Chem. 1984;32:78–80.

5. Climent MJ, Miranda MA. Gas chromatographic-mass spectrometric study of photodegradation of carbamate pesticides. J Chromatogr A. 1996;738:225–31.

6. O. Wuest, W. Meier, Determination of seven carbamate insecticides on fruits and vegetables by capillary gas-chromatography and afid, Zeitschrift Fur Lebensmittel-Untersuchung Und-Forschung, 177 (1983) 25–29.

7. Menezes ML, Felix G. On line extraction and separation of bendiocarb, methomyl, methylparathion, and pentachlorophenol pesticides from raw milk. J Liq Chromatogr Relat Technol. 1998;21:2863–71.

8. Zehner JM, Simonaitis RA, Bry RE. High-performance liquid-chromatographic determination of bendiocarb on wool. J Assoc Off Anal Chem. 1980;63:47–8.

9. Perez-Ruiz T, Martinez-Lozano C, Garcia MD. Determination of N-methylcarbamate pesticides in environmental samples by an automated solid-phase extraction and liquid chromatographic method based on post-column photolysis and chemiluminescence detection. J Chromatogr A. 2007;1164:174–80.

10. Handa SK. Spectrophotometric method for the microdetermination of bendiocarb standard residues in water. J Assoc Off Anal Chem. 1988;71:51–2.

11. Pacioni NL, Veglia AV. Determination of poorly fluorescent carbamate pesticides in water, bendiocarb and promecarb, using cyclodextrin nanocavities and related media. Anal Chim Acta. 2007;583:63–71.

12. Scholz F. Electroanalytical methods: guide to experiments and applications. Berlin: Springer; 2009.

13. Uslu B, Ozkan SA. Electroanalytical methods for the determination of pharmaceuticals: a review of recent trends and developments. Anal Lett. 2011;44:2644–702.

14. Hitchman ML, Ramanathan S. The determination of a carbamate insecticide in soil samples by differential pulse polarography. Anal Chim Acta. 1984;157:349–54.

15. Guiberteau A, Duran-Meras I, Galeano T, Laranjinho TJF, Mora NM, Suarez MF, et al. Voltammetric study of the hydrolysis product of bendiocarb at the glassy carbon electrode. Mikrochim Acta. 2001;137:135–40.

16. Rao TN, Loo BH, Sarada BV, Terashima C, Fujishima A. Electrochemical detection of carbamate pesticides at conductive diamond electrodes. Anal Chem. 2002;74:1578–83.

17. Mirceski V, Komorsky-Lovric S, Lovric M. Square-wave voltammetry: theory and application. Berlin: Springer Science & Business Media; 2007.

18. Luo X, Morrin A, Killard AJ, Smyth MR. Application of nanoparticles in electrochemical sensors and biosensors. Electroanalysis. 2006;18:319–26.

19. Haun JB, Yoon TJ, Lee H, Weissleder R. Magnetic nanoparticle biosensors. Wiley Interdiscip Rev Nanomed Nanobiotechnol. 2010;2:291–304.

20. Luan F, Zhang S, Chen D, Zheng K, Zhuang X. CoS2-decorated ionic liquid-functionalized graphene as a novel hydrazine electrochemical sensor. Talanta. 2018;182:529–35.

21. Zhuang X, Tian C, Luan F, Wu X, Chen L. One-step electrochemical fabrication of a nickel oxide nanoparticle/polyaniline nanowire/ graphene oxide hybrid on a glassy carbon electrode for use as a non-enzymatic glucose biosensor. RSC Adv. 2016;6:92541–6.

22. Zhuang X, Wang H, He T, Chen L. Enhanced voltammetric determination of dopamine using a glassy carbon electrode modified with ionic liquid-functionalized graphene and carbon dots. Microchim Acta. 2016;183:3177–82.

23. Zhuang X, Chen D, Wang S, Liu H, Chen L. Manganese dioxide nanosheet-decorated ionic liquid-functionalized graphene for electrochemical theophylline biosensing. Sensors Actuators B Chem. 2017;251:185–91.

24. Chen D, Zhuang X, Zhai J, Zheng Y, Lu H, Chen L. Preparation of highly sensitive Pt nanoparticles-carbon quantum dots/ionic liquid functionalized graphene oxide nanocomposites and application for H2O2 detection. Sensors Actuators B Chem. 2018;255:1500–6.

25. Zhuang X, Chen D, Zhang S, Luan F, Chen L. Reduced graphene oxide functionalized with a CoS2/ionic liquid composite and decorated with gold nanoparticles for voltammetric sensing of dopamine. Microchim Acta. 2018;185:166.

26. Zhou N, Li J, Chen H, Liao C, Chen L. A functional graphene oxide-ionic liquid composites–gold nanoparticle sensing platform for ultrasensitive electrochemical detection of Hg2+. Analyst. 2013;138:1091–7.

27. Roushani M, Bakyas K, Zare Dizajdizi B. Development of sensitive amperometric hydrogen peroxide sensor using a CuNPs/MB/ MWCNT-C60-Cs-IL nanocomposite modified glassy carbon electrode. Mater Sci Eng C. 2016;64:54–60.

28. Roushani M, Valipour A. Voltammetric immunosensor for human chorionic gonadotropin using a glassy carbon electrode modified with silver nanoparticles and a nanocomposite composed of graphene, chitosan and ionic liquid, and using riboflavin as a redox probe. Microchim Acta. 2016;183:845–53.

29. Roushani M, Valipour A. Using electrochemical oxidation of Rutin in modeling a novel and sensitive immunosensor based on Pt nanoparticle and graphene–ionic liquid–chitosan nanocomposite to detect human chorionic gonadotropin. Sensors Actuators B Chem. 2016;222:1103–11.

30. Roushani M, Shahdost-fard F. A highly selective and sensitive cocaine aptasensor based on covalent attachment of the aptamer-functionalized AuNPs onto nanocomposite as the support platform. Anal Chim Acta. 2015;853:214–21.

31. Gupta AK, Gupta M. Synthesis and surface engineering of iron oxide nanoparticles for biomedical applications. Biomaterials. 2005;26:3995–4021.

32. Lu AH, Salabas EL, Schuth F. Magnetic nanoparticles: synthesis, protection, functionalization, and application. Angew Chem Int Ed. 2007;46:1222–44.

33. Shi X, Gu W, Li B, Chen N, Zhao K, Xian Y. Enzymatic biosensors based on the use of metal oxide nanoparticles. Microchim Acta. 2014;181:1–22.

34. Wu W, He Q, Jiang C. Magnetic iron oxide nanoparticles: synthesis and surface functionalization strategies. Nanoscale Res Lett. 2008;3:397–415.

35. Lin Z, Zhang Z, Li Y, Deng Y. Magnetic nano-Fe3O4 stabilized Pickering emulsion liquid membrane for selective extraction and separation. Chem Eng J. 2016;288:305–11.

36. Yang Z, Shi X, Dai M, Wang L, Xu X, Guo R. Co-metabolic removal of ciprofloxacin under condition of interaction between microbes and Fe3O4. Chem Eng J. 2018;333:649–56.

37. Peng G, Zhang M, Deng S, Shan D, He Q, Yu G. Adsorption and catalytic oxidation of pharmaceuticals by nitrogen-doped reduced graphene oxide/Fe3O4 nanocomposite. Chem Eng J. 2018;341:361–70.

38. Koushkbaghi S, Zakialamdari A, Pishnamazi M, Ramandi HF, Aliabadi M, Irani M. Aminated-Fe3O4 nanoparticles filled chitosan/PVA/PES dual layers nanofibrous membrane for the removal of Cr (VI) and Pb (II) ions from aqueous solutions in adsorption and membrane processes. Chem Eng J. 2018;337:169–82.

39. Kodama RH. Magnetic nanoparticles. J Magn Magn Mater. 1999;200:359–72.

40. Kumar M, Muzzarelli RAA, Muzzarelli C, Sashiwa H, Domb AJ. Chitosan chemistry and pharmaceutical perspectives. Chem Rev. 2004;104:6017–84.

41. Yu C, Gou L, Zhou X, Bao N, Gu H. Chitosan–Fe3O4 nanocomposite based electrochemical sensors for the determination of bisphenol A. Electrochim Acta. 2011;56:9056–63.

42. Kaushik A, Solanki PR, Ansari AA, Sumana G, Ahmad S, Malhotra BD. Iron oxide-chitosan nanobiocomposite for urea sensor. Sensors Actuators B Chem. 2009;138:572–80.

43. Liu X, Zheng S, Hu Y, Li Z, Luo F, He Z. Electrochemical immunosensor based on the chitosan-magnetic nanoparticles for detection of tetracycline. Food Anal Methods. 2016;9:2972–8.

44. Wang Y-H, Yu C-M, Gu H-Y, Tu Y-F. The hemoglobin-modified electrode with chitosan/Fe3O4 nanocomposite for the detection of trichloroacetic acid. J Solid State Electrochem. 2016;20:1337–44.

45. Ran G, Chen X, Xia Y. Electrochemical detection of serotonin based on a poly (bromocresol green) film and Fe3O4 nanoparticles in a chitosan matrix. RSC Adv. 2017;7:1847–51.

46. Dehdashtian S, Gholivand MB, Shamsipur M, Kariminia S. Construction of a sensitive and selective sensor for morphine using chitosan coated Fe3O4 magnetic nanoparticle as a modifier. J Mater Chem A. 2016;58:53–9.

47. Freire TM, Dutra LMU, Queiroz DC, Ricardo NMPS, Barreto K, Denardin JC, et al. Fast ultrasound assisted synthesis of chitosan-based magnetite nanocomposites as a modified electrode sensor. Carbohydr Polym. 2016;151:760–9.

48. Oliveira TMBF, Ribeiro FWP, do Nascimento JM, Soares JES, Freire VN, Becker H, et al. Direct electrochemical analysis of dexamethasone endocrine disruptor in raw natural waters. J Braz Chem Soc. 2012;23:110–9.

49. Sousa CP, Salvador MA, Homem-de-Mello P, Ribeiro FWP, de Lima-Neto P, Correia AN. Computational modeling of functionalized multi-walled carbon nanotubes dispersed in polyethylenimine for electrochemical sensing of acetaminophen. Sensors Actuators B Chem. 2017;246:969–78.

50. Warner J, Engel T, Mondron P. Determination of bendiocarb in industrial and municipal wastewaters. Washington, D.C.: US Environ. Prot. Agency; 1985. EPA/600/4-85/021.

51. C. Analytical Methods. Recommendations for the definition, estimation and use of the detection limit. Analyst. 1987;112:199–204.

52. Mocak J, Bond A, Mitchell S, Scollary G. A statistical overview of standard (IUPAC and ACS) and new procedures for determining the limits of detection and quantification: application to voltammetric and stripping techniques (technical report). Pure Appl Chem. 1997;69:297–328.

53. Oliveira TMBF, Becker H, Longhinotti E, De Souza D, de Lima-Neto P, Correia AN. Carbon-fibre microelectrodes coupled with square-wave voltammetry for the direct analysis of dimethomorph fungicide in natural waters. Microchem J. 2013;109:84–92.

54. Bard AJ, Faulkner LR. Electrochemical methods: fundamentals and applications. Wiley; 2000.

55. Urbanova V, Magro M, Gedanken A, Baratella D, Vianello F, Zboril R. Nanocrystalline iron oxides, composites, and related materials as a platform for electrochemical, magnetic, and chemical biosensors. Chem Mater. 2014;26:6653–73.

56. Sharma G, Kumar D, Kumar A, Al-Muhtaseb AH, Pathinia D, Naushad M, et al. Revolution from monometallic to trimetallic nanoparticle composites, various synthesis methods and their applications: a review. J Mater Chem A. 2017;71:1216–30.

57. Sousa CP, de Oliveira RC, Freire TM, Fechine PBA, Salvador MA, Homem-de-Mello P, et al. Chlorhexidine digluconate on chitosan-magnetic iron oxide nanoparticles modified electrode: electroanalysis and mechanistic insights by computational simulations. Sensors Actuators B Chem. 2017;240:417–25.

58. Li X, Li Y, Li S, Zhou W, Chu H, Chen W, et al. Single crystalline trigonal selenium nanotubes and nanowires synthesized by sonochemical process. Cryst Growth Des. 2005;5:911–6.

59. Neto DMA, Freire RM, Gallo J, Freire TM, Queiroz DC, Ricardo NMPS, et al. Rapid sonochemical approach produces functionalized Fe3O4 nanoparticles with excellent magnetic, colloidal, and relaxivity properties for MRI application. J Phys Chem C. 2017;121:24206–22.

60. Singh AK, Srivastava ON, Singh K. Shape and size-dependent magnetic properties of Fe3O4 nanoparticles synthesized using piperidine. Nanoscale Res Lett. 2017;12:298.

61. Compton RG, Banks CE. Understanding voltammetry. World Scientific; 2007.

62. Croucher L, Jewess P, Roberts MC. Metabolic pathways of agrochemicals: part 2: insecticides and fungicides. Royal Society of Chemistry; 2007.

63. Skládal P. Determination of organophosphate and carbamate pesticides using a cobalt phthalocyanine-modified carbon paste electrode and a cholinesterase enzyme membrane. Anal Chim Acta. 1991;252:11–5.

64. Kumar KS, Suvardhan K, Rekha D, Kiran K, Jayaraj B, Janardhanam K, et al. Development of simple and sensitive spectrophotometric method for the determination of bendiocarb in its formulations and environmental samples. Environ Monit Assess. 2007;127:67–72.

65. Jarvie HP, Sharpley AN, Withers PJA, Scott JT, Haggard BE, Neal C. Phosphorus mitigation to control river eutrophication: murky waters, inconvenient truths, and "postnormal" science. J Environ Qual. 2013;42:295–304.

66. Petersen CR, Jovanovic NZ, Grenfell MC, Oberholster PJ, Cheng P. Responses of aquatic communities to physical and chemical parameters in agriculturally impacted coastal river systems. Hydrobiologia. 2018;813:157–75.